



Contents lists available at ScienceDirect

Bioorganic & Medicinal Chemistry

journal homepage: www.elsevier.com/locate/bmc

Identification of nitroimidazole-oxime derivatives targeting the polo-box domain of polo-like kinase 1

Juan Sun^{a,b,*}, Han-Yu Liu^a, Ruo-Fei Xu^c, Hai-Liang Zhu^{b,*}

^aSchool of Life Sciences, Shandong University of Technology, Zibo 255049, PR China

^bElion Nature Biological Technology Co., Ltd, Nanjing 210046, PR China

^cShandong Experimental High School, Jinan 250001, PR China

ARTICLE INFO

Article history:

Received 18 July 2017

Revised 15 October 2017

Accepted 25 October 2017

Available online xxxx

Keywords:

Nitroimidazole-oxime

PLK1-PBD

Antitumor

Molecular docking

ABSTRACT

Recent progress in the development of small molecular skeleton-derived polo-like kinase (PLK1) catalytic domain (K_D) inhibitors has led to the synthesis of multiple ligands with high binding affinity. However, few systematic analyses have been conducted to identify key PLK1-PBD domain and characterize their interactions with potent PLK1 inhibitors. Therefore, we designed a series of PLK1-PBD inhibitors with an *in silico* scaffold modification strategy. A docking simulation combined with a primary screen *in vitro* were performed to filter for the lead compound, which was then substituted, synthesized and evaluated by a variety of bioassays. The biological profile of **4v** suggests that this compound may be developed as a potential anticancer agent.

© 2017 Elsevier Ltd. All rights reserved.

1. Introduction

Polo-like kinase 1 (PLK1), a key player in mitosis,^{1,2} modulates the transition through the G2/M checkpoint, is crucial in cell proliferation and has been considered as a target for tumor therapy.^{3,4} Until now, two distinct drug targets have been identified in PLK1: a N-terminal catalytic domain (K_D) and a C-terminal domain having 2 highly homologous sequences, termed polo-box domain (PBD). For a long period, discovery of PLK1 inhibitors has been focused on targeting the N-terminal catalytic domain.^{5,6} However, protein kinases have high similarities in the ATP-binding pockets,⁷ and these efforts suffered from a lack of specificity. An alternative approach with potential for identifying potent and highly selective kinase inhibitors is to target the interfaces of protein-protein complexes of interest.⁸ Therefore, the special structure of the PBD has become an highly selective target.^{9,10}

Several series of peptides were designed and synthesized targeting PLK1-PBD with high affinity and specificity.^{11–16} However, inadequate proteolytic resistance and cell permeability of the peptides hinder the development of these peptide-based inhibitors into novel therapeutic compounds. In order to overcome the shortcomings of peptide-based inhibitors, some small molecules have been designed and synthesized targeting PLK1-PBD.^{17–22} Unfortu-

nately, the limited number of PLK1-PBD inhibitors and their modest selectivity greatly limit the design based on the structure. Therefore, clarifying the binding mode between PBD and small molecules, as well as improving their specificity recognition, is the key issues to be resolved.

To continue our efforts aimed at discovering and developing PLK1-PBD inhibitors²³, in this study, we used a structure-based approach to design a novel and potent small molecule named **4v**, which exhibits a high binding affinity for PLK1-PBD.

2. Results and discussion

2.1. Structure-based design of small molecules

To identify the minimal set of key residues required for a high binding affinity, we examined the previously reported cocrystal structures of PLK1-PBD²⁴ (PDB ID: 4HCO) in complex with a ligand. Then we have found that three binding pockets are critical to bind PLK1-PBD with high affinity, combined with our previous research²³: (1) Electrostatic-binding region (EBR) in which the Lys540-His538 pincer clinches phosphopeptides by the phosphate. (2) Hydrogen-bonding region (HBR) is surrounded by Trp414, Phe535 and Arg516 residues through participating in a hydrogen bonding interactions. (3) Hydrophobic motif (HM) formed by Val415, Tyr417, Tyr485 and Leu490 through hydrophobic interactions with the above residues (Fig. 1). These observations suggest

* Corresponding authors at: School of Life Sciences, Shandong University of Technology, Zibo 255049, PR China (J. Sun).

E-mail address: sunreiyi86@163.com (J. Sun).

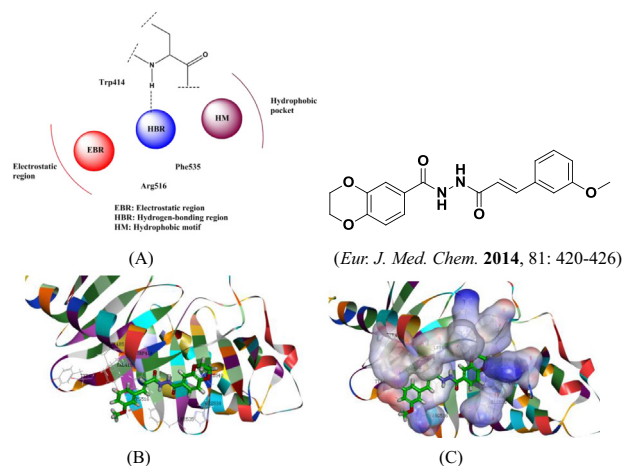


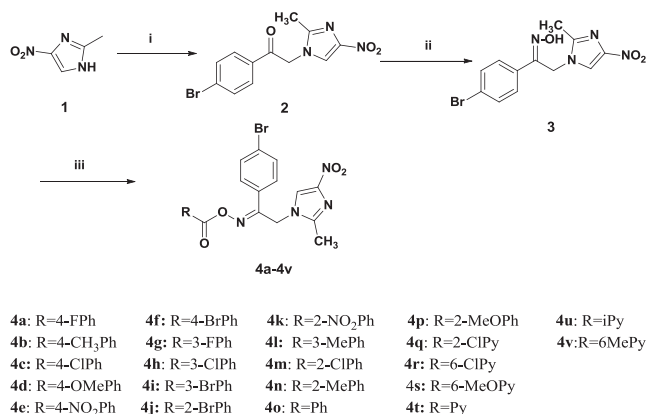
Fig. 1. Three binding pockets are critical to bind PLK1-PBD with high affinity: (A) 2D figure. (B) 3D figure. (C) 3D figure.

that appropriate design of small molecules would provided drug-like small molecule targeting PLK1-PBD with high binding affinity.

According to our previous research and the three binding pockets, we have selected benzene ring and pyridine ring as the basic scaffold. At the same time, a variety of substituents have been introduced, aim to investigate the position effect, space effect, electron effect, hydrophilicity and hydrophobicity against to the biological activity of the target compounds. Meanwhile, nitroimidazole-oxime skeleton has a good affinity with Lys540-His538 pincer clinches in the EBR region according to the Docking simulations. Therefore, in this research, we presented a nitroimidazole-oxime as our scaffold which provides rigidity around the central unit.

2.2. Chemistry

Twenty-two nitroimidazole-oxime analogs were synthesized and all of them were synthesized for the first time. The synthesis of compounds has been followed the general pathway outlined in Scheme 1. All of the synthetic compounds **4a–4v** are being reported for the first time and gave satisfactory analytical and spectroscopic data.



Scheme 1. General synthesis of compounds **4a–4v**. Reagents and conditions: (i) 2,4'-dibromo-acetophenone, K₂CO₃, TBAB, ethanol, reflux, 0.5–1 h. (ii) Hydroxylamine hydrochloride, K₂CO₃, ethanol, reflux, 2–4 h. (iii) Substituted benzoic acid, niacin or isonicotinic acid, EDC·HCl, HoBT, rt, 8–10 h.

Table 1
In vitro anticancer activities against four human tumor cell lines.

Compounds	IC ₅₀ ± SD (μg/mL)			
	MGC-803	HepG-2	MCF-7	Hela
3	>20	17.39 ± 0.12	>20	>20
4a	1.24 ± 0.05	1.22 ± 0.08	2.12 ± 0.03	7.24 ± 0.06
4b	0.81 ± 0.03	0.96 ± 0.02	1.54 ± 0.05	0.96 ± 0.02
4c	0.45 ± 0.02	1.34 ± 0.05	2.79 ± 0.07	8.79 ± 0.03
4d	0.34 ± 0.04	1.25 ± 0.07	3.15 ± 0.02	6.54 ± 0.04
4e	0.37 ± 0.02	1.43 ± 0.09	0.86 ± 0.03	12.41 ± 0.19
4f	1.48 ± 0.06	2.56 ± 0.04	2.56 ± 0.05	5.67 ± 0.06
4g	0.21 ± 0.03	0.97 ± 0.02	1.87 ± 0.03	4.55 ± 0.04
4h	0.18 ± 0.02	1.15 ± 0.03	0.84 ± 0.06	4.09 ± 0.04
4i	0.04 ± 0.01	0.86 ± 0.05	1.37 ± 0.02	2.57 ± 0.08
4j	2.63 ± 0.87	4.38 ± 0.01	3.79 ± 0.09	>20
4k	2.54 ± 0.04	6.59 ± 0.5	7.13 ± 0.04	11.35 ± 0.07
4l	3.25 ± 0.02	10.65 ± 0.14	2.82 ± 0.03	12.35 ± 0.09
4m	0.16 ± 0.07	1.33 ± 0.05	1.27 ± 0.08	8.53 ± 0.06
4n	0.84 ± 0.06	2.37 ± 0.02	2.15 ± 0.06	9.76 ± 0.05
4o	3.66 ± 0.05	13.96 ± 0.28	>20	>20
4p	3.53 ± 0.04	>20	3.13 ± 0.07	>20
4q	0.73 ± 0.05	0.76 ± 0.03	0.76 ± 0.04	1.28 ± 0.01
4r	0.82 ± 0.03	0.71 ± 0.02	0.79 ± 0.02	0.96 ± 0.02
4s	0.03 ± 0.01	0.92 ± 0.03	0.89 ± 0.02	2.35 ± 0.04
4t	0.01 ± 0.01	0.73 ± 0.01	0.78 ± 0.03	1.51 ± 0.05
4u	0.02 ± 0.01	0.81 ± 0.02	0.87 ± 0.01	1.63 ± 0.02
4v	0.005 ± 0.003	0.75 ± 0.01	0.72 ± 0.02	0.86 ± 0.03
5-FU	1.8 ± 0.02	2.24 ± 0.07	2.19 ± 0.03	3.82 ± 0.08

2.3. MTT assay for cell proliferation

To test the antiproliferative activities of the synthesized compounds, the target compounds were evaluated *in vitro* antiproliferation assays against four human cancer cell lines (MCF7, HeLa, MGC803 and HepG2). The results were summarized in Table 1. With few exception, the active analogs showed a remarkable potential antiproliferative activity against MGC803 (Fig. 2), suggesting that nitroimidazole-oxime derivatives could significantly enhance antiproliferative potency. For the given compounds, it was observed that compound **4v** showed the most potent antiproliferative activity (IC₅₀ = 0.002 μg/mL).

Structure–activity relationship (SAR) analysis indicated that different acids substitutes led to different antitumor activity, and the potency order was niacin > benzoic acid. compounds **4q** and **4r** with substituted Cl group on niacin ring showed moderate antitumor activity with IC₅₀ of 0.71–1.28 μg/mL against four human cancer cell lines. Based on the data obtained, compounds **4t** and **4u** with niacin and Isonicotinic ring were found to be better activity toward BGC823 cancer cell line with IC₅₀ values, 0.01 and 0.02 μg/mL respectively.

2.4. Cytotoxicity test

Generally speaking, the inhibitory activity of the compounds is due to cell apoptosis or toxic effect, so we performed cytotoxicity test before detecting kinase activity. All of the compounds were detected for their cytotoxicity on Human Kidney epithelia cells (293T). The pharmacological results of these compounds were summarized in Table 2. What we can see from the data is that most of the compounds were low toxic.

2.5. PLK1-PBD inhibitory assay

To validate whether the above anti-proliferative effect was produced by interaction of PLK1 protein and the synthesized compounds, the selected compounds were evaluated for their abilities to inhibit the activity of PLK1 protein kinases relevant to cancer. As expected, all compounds displayed the best inhibitory

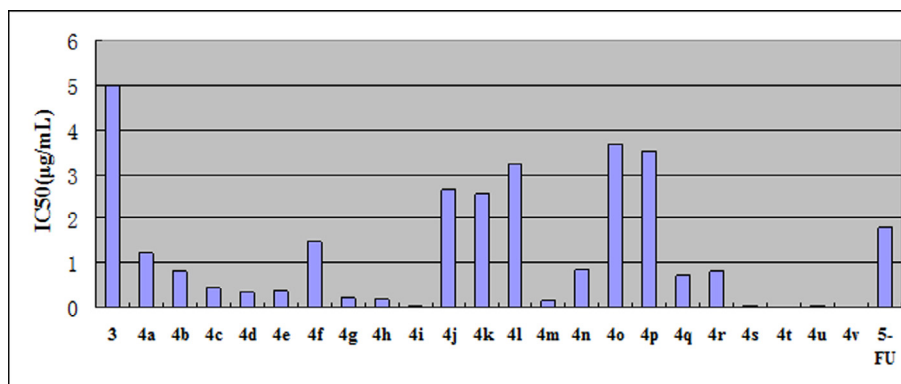


Fig. 2. The inhibition rates of synthesized compounds on MGC803.

Table 2
Cell proliferation assay on 293T and kinase inhibitory activities (µg/ml).

Compounds	CC ₅₀	PLK1-PBD
4a	2.3×10^4	0.69 ± 0.12
4b	2.7×10^2	0.23 ± 0.03
4c	2.3×10^2	0.17 ± 0.11
4d	1.6×10^3	0.22 ± 0.02
4e	1.6×10^2	0.1 ± 0.02
4f	3.3×10^2	0.88 ± 0.31
4g	5.3×10^2	0.11 ± 0.01
4h	7.0×10^2	0.13 ± 0.02
4i	1.8×10^2	0.18 ± 0.02
4j	1.5×10^2	1.66 ± 0.22
4k	2.3×10^2	1.95 ± 0.31
4l	1.3×10^3	2.88 ± 0.01
4m	5.3×10^2	0.33 ± 0.07
4n	3.8×10^3	0.25 ± 0.01
4o	3.2×10^4	3.15 ± 0.40
4p	5.0×10^2	2.93 ± 0.22
4q	1.2×10^4	0.25 ± 0.09
4r	2.5×10^2	0.28 ± 0.03
4s	9.8×10^2	0.05 ± 0.02
4t	0.5×10^2	0.03 ± 0.01
4u	0.8×10^2	0.06 ± 0.02
4v	8.3×10^3	0.002 ± 0.02
Thymoquinone	1.4×10^2	2.19 ± 0.03

activity for PLK1 and the results have been showed in Table 2. Besides, a further study between the anti-proliferative activity against MGC803 cell line and the PLK1 inhibitory activity of these compounds was analyzed and the result indicated that there was a moderate correlation between PLK1 inhibition and inhibition of cancer cellular proliferation, as evidenced in Fig. 3. The correlation coefficient r^2 was found to be 0.691.

2.6. Annexin V-FITC/PI apoptosis detection

Besides, we detected the mechanism of compound 4v inhibition activity by flow cytometry (FCM) (Fig. 4) and found that the compound could induce the apoptosis of activated MGC803 cells in a dose-dependent manner. As shown in Fig. 4, MGC803 cells were treated with 0.01, 0.06 and 0.12 µM of compound 4v for 24 h. The compound increased the percentage of apoptosis by Annexin V-FITC/PI staining in a dose-dependent.

2.7. Docking simulations

Docking study was performed to fit compound 4v into the active center of the polo-box domain of polo-like kinase 1 (PDB code: 4HCO). The obtained results were presented in Fig. 5(A). In the binding model, compound 4v is nicely bound to the active site

PBD domain of PLK1 by three hydrogen bonds with Lys540 and Arg 557, one *Pi*-cation bond with Lys540, and one *Pi-Pi* bond with Trp 414. Nitroimidazole group has a good affinity with Lys540-His538 pincer clinches in the EBR region, and 6-methoxypyridine group is perfectly fit in the HM region. Furthermore, other weak interactions, such as Vander Waals and carbon-hydrogen bonds, also contributed to the binding affinity of 4v with PLK1. In Fig. 5(B), 3D models are depicted. The molecular docking suggests that compound 4v maybe a potential PLK1-PBD ligand.

2.8. Single crystal X-ray diffraction

Crystals of compound 4t (CCDC 1487468) were obtained from methanol solution. Fig. 6A shows a perspective view of the monomeric unit with the atomic numbering scheme, and Fig. 6B depicts the intramolecular and intermolecular hydrogen bonds. Crystallographic data, details of data collection and structure refinement parameters are listed in Table 3. The hydrogen bond lengths and bond angles are given in Table 4.

3. Conclusions

In this study, a series of nitroimidazole-oxime derivatives were designed as new PLK1-PBD inhibitors based on the computer-aided drug design. These compounds were tested in a series of experiments and the results indicated that some compounds may be promising in drug development. Compound 4v is the most impressive, with a notable biological profile. Against PLK1-PBD and the MGC803 cancer cell line, 4v demonstrated better inhibitory potency than poloxin. Assisted by apoptosis of MGC803 cell, 4v could induce apoptosis in a dose-dependent manner. We hope that this study will benefit the study of cancer treatment through PLK1-PBD inhibition.

4. Experimental results

4.1. Chemistry

All chemicals (reagent grade) used were purchased from Aladdin (Shanghai, China). All the ¹H NMR spectra were recorded on a Bruker DPX 400 model spectrometer in DMSO *d*₆, and chemical shifts (δ) are reported as parts per million (ppm). ESI-MS spectra were recorded by a Mariner System 5304 Mass spectrometer. Melting points were determined on a Digital Melting Point apparatus (Shenguang., Shanghai, China). Thin layer chromatography (TLC) was performed on silica gel plates (Silica Gel 60 GF254) and visualized in UV light (254 nm and 365 nm). The PLK1 Kinase Assay Kit was purchased from Bio-Swamp.

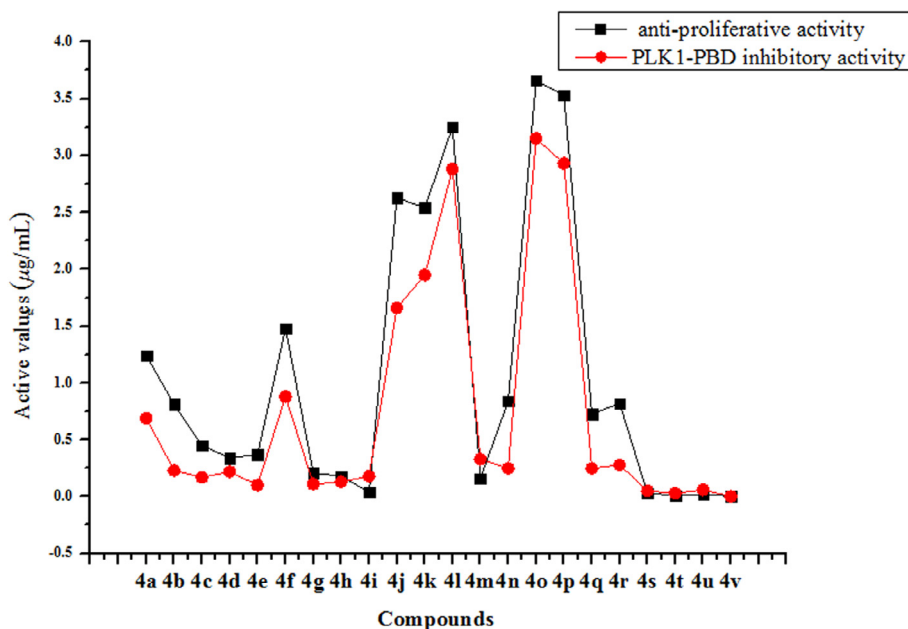


Fig. 3. Correlation between the anti-proliferative activity against MGC-803 and the PLK1-PBD inhibitory activity, which indicated that there was a moderate correlation between PLK1-PBD inhibition and inhibition of cellular proliferation.

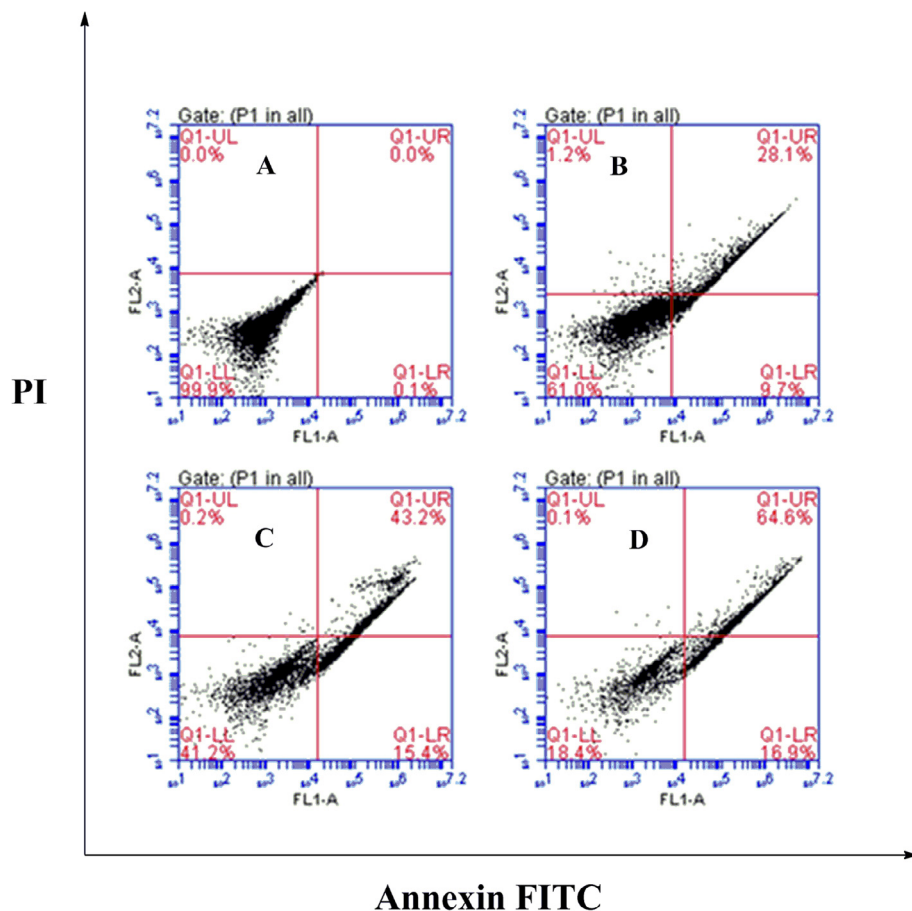


Fig. 4. MGC803 cells were cultured with anticancer and various concentrations of 4v for 24 h. Cells were stained by Annexin V/FITC/PI and apoptosis was analyzed by flow cytometry. (A) Control. (B) 0.01 µM. (C) 0.06 µM. (D) 0.12 µM.

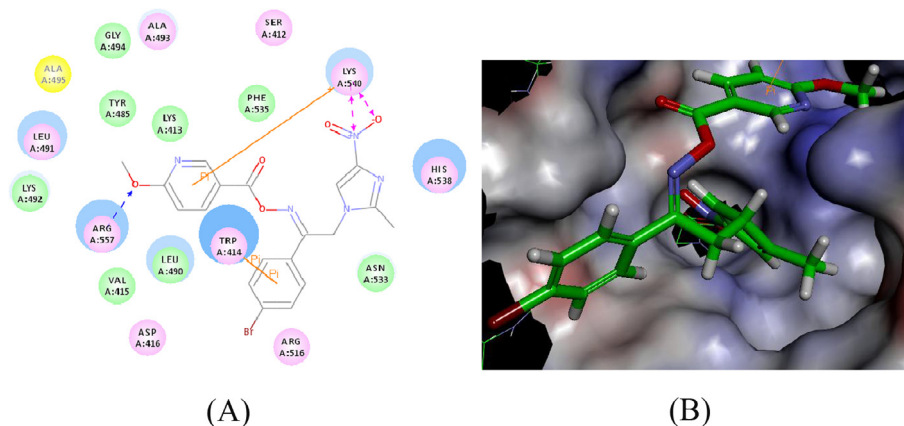


Fig. 5. (A) 2D molecular docking model of compound **4v** with 4HCO. (B) 3D interaction map between compound **4v** and 4HCO binding site.

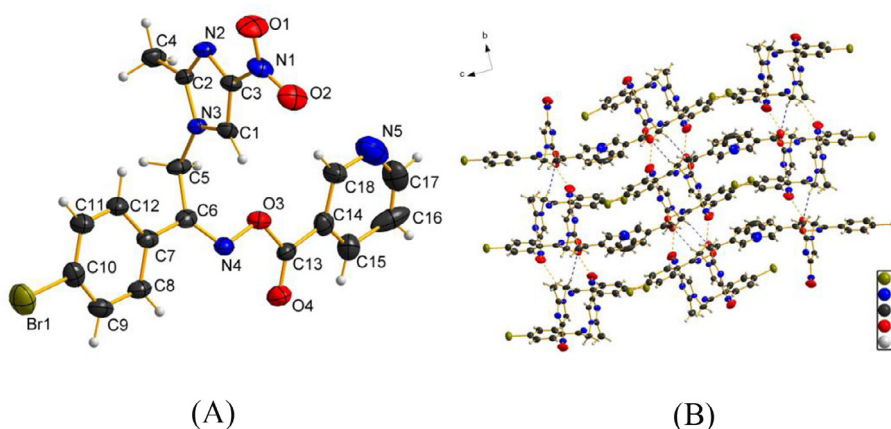


Fig. 6. Crystal structure of compound **4t**. (A) Molecular structure of compound **4t** with atomic numbering scheme. (B) Crystal packing of the compound **4t**.

4.2. General procedure for the synthesis of compounds **4a–4v**

Commercially available 2-methyl-4-nitroimidazole, potassium carbonate and tetrabutylammonium bromide were reacted with 2,4'-dibromo-acetophenone in ethanol to give compound **2**. Compound **2** was reacted with hydroxylamine hydrochloride in ethanol to give compound **3**. Then target compound **4a–4v** were obtained with proper substituted benzoic acid or niacin under the condition of EDCI and HoBt in CH_2Cl_2 .

4.2.1. 1-(4-Bromophenyl)-2-(2-methyl-4-nitro-1H-imidazol-1-yl) ethanone-(4-fluorobenzoyl)oxime (**4a**)

White crystal, yield 92%, m.p. 171.4–172.2 °C. ^1H NMR (400 MHz, $\text{DMSO-}d_6$) δ (ppm): 8.194 (s, 1H), 7.712–7.690 (m, 1H), 7.649–7.558 (m, 5H), 7.259–7.101 (m, 1H), 6.393–6.372 (m, 1H), 5.417 (s, 2H), 2.510–2.502 (m, 3H). MS (ESI): 463.02 ($\text{C}_{19}\text{H}_{15}\text{BrFN}_4\text{O}_4$, $[\text{M}+\text{H}]^+$). Anal. Calcd: C, 49.48; H, 3.06; N, 12.15%; Found: C, 49.42; H, 3.11; N, 12.05%.

4.2.2. 1-(4-Bromophenyl)-2-(2-methyl-4-nitro-1H-imidazol-1-yl) ethanone-(4-methylbenzoyl)oxime (**4b**)

White crystal, yield 84%, m.p. 171.4–171.5 °C. ^1H NMR (400 MHz, $\text{DMSO-}d_6$) δ (ppm): 7.419 (s, 1H), 7.276 (s, 5H), 7.243–7.146 (m, 3H), 5.163 (s, 2H), 2.764–2.735 (m, 2H), 2.578–2.565 (m, 1H), 2.329–2.247 (m, 3H). MS (ESI): 457.04 ($\text{C}_{20}\text{H}_{18}\text{BrN}_4\text{O}_4$, $[\text{M}+\text{H}]^+$). Anal. Calcd: C, 52.53; H, 3.75; N, 12.25%; Found: C, 52.19; H, 3.14; N, 12.09%.

4.2.3. 1-(4-Bromophenyl)-2-(2-methyl-4-nitro-1H-imidazol-1-yl) ethanone-(4-chlorobenzoyl)oxime (**4c**)

White crystal, yield 87%, m.p. 170.4 °C. ^1H NMR (400 MHz, $\text{DMSO-}d_6$) δ (ppm): 8.374 (s, 1H), 8.289–8.253 (m, 2H), 7.947–7.918 (m, 1H), 7.620–7.537 (m, 4H), 7.254–7.183 (m, 1H), 5.638

Table 3

Crystallographic data, details of data collection and structure refinement parameters.

compound	4t
Empirical formula	$\text{C}_{18}\text{H}_{14}\text{BrN}_5\text{O}_4$
Formula weight	444.24
Crystal system	Orthorhombic
Space group	P_{bca} (No. 61)
a (Å)	10.6734(8)
b (Å)	15.7179(13)
c (Å)	22.2989(16)
α (°)	90
β (°)	90
γ (°)	90
V (Å ³)	3740.9(5)
Z	8
F(0 0 0)	1792
Dx(g/cm ³)	1.578
Mu(MoKa) [1/mm]	2.233
GOOF	1.07
R _{int}	0.0596
R ₁ ; wR ₂ [I > 2σ(I)]	0.0833, 0.2321
R ₁ ; wR ₂ (all data)	0.1313, 0.2633
θ range (°)	2.5–25.1
T (K)	273

Table 4
Hydrogen bond lengths (Å) and bond angles (°) of compound **4t**.

H-bond type	Symmetry code	D–H...A	d(D–H)	d(H...A)	d(D...A)	∠DHA
Inter	1 – x, 1 – y, 2 – z	C4–H4C...O4	0.96	2.60	3.469(8)	151
	1/2 – x, –1/2 + y, z	C5–H5A...O4	0.97	2.57	3.431(9)	148
	1 + x, y, z	C5–H5B...O2	0.97	2.37	3.176(8)	140
	1/2 + x, 1/2 – y, 2 – z	C12–H12...N2	0.93	2.58	3.337(8)	138
Intra	–	C5–H5B...O3	0.97	2.23	2.599(7)	101

(s, 2H), 2.449–2.351 (s, 3H). MS (ESI): 478.99 (C₁₉H₁₅BrClN₄O₄, [M+H]⁺). Anal. Calcd: C, 47.77; H, 2.95; N, 11.73%; Found: C, 47.18; H, 3.06; N, 11.68%.

4.2.4. 1-(4-bromophenyl)-2-(2-methyl-4-nitro-1H-imidazol-1-yl) ethanone-(4-methoxy-benzoyl)oxime (4d)

White crystal, yield 85%, m.p. 172.0–172.7 °C. ¹H NMR (400 MHz, DMSO *d*₆) δ (ppm): 8.357–8.302 (m, 1H), 8.117–8.088 (d, *J* = 11.6 Hz, 1H), 7.797–7.590 (m, 5H), 7.124–7.017 (m, 2H), 5.824 (s, 2H), 3.880–3.814 (m, 3H), 2.412–2.249 (m, 3H). MS (ESI): 475.04 (C₂₀H₁₈BrN₄O₅, [M+H]⁺). Anal. Calcd: C, 50.76; H, 3.62; N, 11.84%; Found: C, 50.69; H, 3.57; N, 11.59%.

4.2.5. 1-(4-Bromophenyl)-2-(2-methyl-4-nitro-1H-imidazol-1-yl) ethanone-(4-nitro-benzoyl)oxime (4e)

Yellow crystal, yield 94%, m.p. 171.1–171.6 °C. ¹H NMR (400 MHz, DMSO *d*₆) δ (ppm): 8.410 (s, 1H), 8.374–8.356 (m, 1H), 8.274–8.231 (m, 2H), 7.711–7.431 (m, 5H), 5.871–5.844 (m, 2H), 2.511–2.502 (m, 3H). MS (ESI): 488.01 (C₁₉H₁₅BrN₅O₆, [M+H]⁺). Anal. Calcd: C, 46.74; H, 2.89; N, 14.34%; Found: C, 46.82; H, 2.83; N, 14.29%.

4.2.6. 1-(4-Bromophenyl)-2-(2-methyl-4-nitro-1H-imidazol-1-yl) ethanone-(4-bromo-benzoyl)oxime (4f)

White crystal, yield 92%, m.p. 171.0–171.3 °C. ¹H NMR (400 MHz, DMSO *d*₆) δ (ppm): 8.137–8.105 (m, 2H), 7.976–7.939 (m, 1H), 7.759–7.743 (m, 2H), 7.626–7.558 (m, 4H), 5.833 (s, 2H), 2.451–2.419 (m, 3H). MS (ESI): 522.94 (C₁₉H₁₅Br₂N₄O₄, [M+H]⁺). Anal. Calcd: C, 43.70; H, 2.70; N, 10.73%; Found: C, 43.61; H, 2.81; N, 10.65%.

4.2.7. 1-(4-Bromophenyl)-2-(2-methyl-4-nitro-1H-imidazol-1-yl) ethanone-(3-fluoro-benzoyl)oxime (4g)

White crystal, yield 91%, m.p. 171.7–172.1 °C. ¹H NMR (400 MHz, DMSO *d*₆) δ (ppm): 8.584 (s, 1H), 8.359 (s, 1H), 8.213–7.992 (m, 1H), 7.719–7.658 (m, 4H), 7.396–7.349 (m, 2H), 5.687–5.647 (m, 2H), 2.519–2.428 (m, 3H). MS (ESI): 463.02 (C₁₉H₁₅BrFN₄O₄, [M+H]⁺). Anal. Calcd: C, 49.48; H, 3.06; N, 12.15%; Found: C, 49.56; H, 3.11; N, 12.01%.

4.2.8. 1-(4-Bromophenyl)-2-(2-methyl-4-nitro-1H-imidazol-1-yl) ethanone-(3-chloro-benzoyl)oxime (4h)

White crystal, yield 95%, m.p. 170.7–170.8 °C. ¹H NMR (400 MHz, DMSO *d*₆) δ (ppm): 8.381 (s, 1H), 8.132–8.093 (m, 2H), 7.849–7.819 (m, 1H), 7.710–7.667 (m, 2H), 7.641–7.589 (m, 3H), 5.871 (s, 2H), 2.247 (s, 3H). MS (ESI): 478.99 (C₁₉H₁₅BrClN₄O₄, [M+H]⁺). Anal. Calcd: C, 47.77; H, 2.95; N, 11.73%; Found: C, 47.68; H, 3.08; N, 11.59%.

4.2.9. 1-(4-Bromophenyl)-2-(2-methyl-4-nitro-1H-imidazol-1-yl) ethanone-(3-bromo-benzoyl)oxime (4i)

White crystal, yield 92%, m.p. 172.7–172.8 °C. ¹H NMR (400 MHz, DMSO *d*₆) δ (ppm): 8.412 (s, 1H), 8.272–8.264 (m, 1H), 8.272–8.152 (d, *J* = 8.0 Hz, 1H), 7.987–7.967 (d, *J* = 8.0 Hz, 1H), 7.712–7.690 (m, 2H), 7.612–7.559 (m, 3H), 5.885 (s, 2H), 2.511–

2.502 (m, 3H). MS (ESI): 522.94 (C₁₉H₁₅Br₂N₄O₄, [M+H]⁺). Anal. Calcd: C, 43.70; H, 2.70; N, 10.73%; Found: C, 43.59; H, 2.79; N, 10.65%.

4.2.10. 1-(4-Bromophenyl)-2-(2-methyl-4-nitro-1H-imidazol-1-yl) ethanone-(2-bromo-benzoyl)oxime (4j)

White crystal, yield 92%, m.p. 170.7 °C. ¹H NMR (400 MHz, DMSO *d*₆) δ (ppm): 8.289 (s, 1H), 7.936–7.905 (m, 1H), 7.853–7.822 (m, 1H), 7.717–7.688 (m, 2H), 7.635–7.558 (m, 4H), 5.781 (s, 2H), 2.251–2.210 (m, 3H). MS (ESI): 522.94 (C₁₉H₁₅Br₂N₄O₄, [M+H]⁺). Anal. Calcd: C, 43.70; H, 2.70; N, 10.73%; Found: C, 43.59; H, 2.61; N, 10.84%.

4.2.11. 1-(4-Bromophenyl)-2-(2-methyl-4-nitro-1H-imidazol-1-yl) ethanone-(2-nitro-benzoyl)oxime (4k)

Yellow crystal, yield 93%, m.p. 158.5–158.6 °C. ¹H NMR (400 MHz, DMSO *d*₆) δ (ppm): 8.763 (s, 1H), 8.572–8.534 (m, 1H), 8.375–8.341 (m, 3H), 7.951–7.894 (m, 4H), 5.843–5.823 (m, 2H), 2.591–2.578 (m, 3H). MS (ESI): 488.01 (C₁₉H₁₅BrN₅O₆, [M+H]⁺). Anal. Calcd: C, 46.74; H, 2.89; N, 14.34%; Found: C, 46.59; H, 3.01; N, 14.42%.

4.2.12. 1-(4-Bromophenyl)-2-(2-methyl-4-nitro-1H-imidazol-1-yl) ethanone-(3-methylbenzoyl)oxime (4l)

White crystal, yield 90%, m.p. 159.5–159.6 °C. ¹H NMR (400 MHz, DMSO *d*₆) δ (ppm): 8.580–8.558 (m, 1H), 8.423–8.407 (m, 3H), 8.098–8.078 (m, 3H), 7.634–7.612 (m, 2H), 5.896 (s, 2H), 3.353–3.330 (m, 3H), 2.260 (s, 3H). MS (ESI): 457.04 (C₂₀H₁₈BrN₄O₄, [M+H]⁺). Anal. Calcd: C, 52.53; H, 3.75; N, 12.25%; Found: C, 52.62; H, 3.65; N, 12.14%.

4.2.13. 1-(4-Bromophenyl)-2-(2-methyl-4-nitro-1H-imidazol-1-yl) ethanone-(2-chloro-benzoyl)oxime (4m)

White crystal, yield 91%, m.p. 170.7–170.8 °C. ¹H NMR (400 MHz, DMSO *d*₆) δ (ppm): 8.543 (s, 1H), 8.173–8.157 (m, 1H), 8.134–8.121 (m, 1H), 7.839–7.812 (m, 3H), 7.356–7.235 (m, 3H), 6.247 (s, 2H), 2.168–2.139 (m, 3H). MS (ESI): 478.99 (C₁₉H₁₅BrClN₄O₄, [M+H]⁺). Anal. Calcd: C, 47.77; H, 2.95; N, 11.73%; Found: C, 47.91; H, 3.08; N, 11.62%.

4.2.14. 1-(4-Bromophenyl)-2-(2-methyl-4-nitro-1H-imidazol-1-yl) ethanone-(2-methylbenzoyl)oxime (4n)

White crystal, yield 92%, m.p. 171.0–171.5 °C. ¹H NMR (400 MHz, DMSO *d*₆) δ (ppm): 8.359 (s, 1H), 7.713–7.692 (m, 2H), 7.613–7.567 (m, 4H), 7.439–7.383 (m, 2H), 5.763 (s, 2H), 2.569–2.506 (m, 3H), 2.245–2.222 (m, 3H). MS (ESI): 457.04 (C₂₀H₁₈BrN₄O₄, [M+H]⁺). Anal. Calcd: C, 52.53; H, 3.75; N, 12.25%; Found: C, 52.65; H, 3.62; N, 12.31%.

4.2.15. 1-(4-Bromophenyl)-2-(2-methyl-4-nitro-1H-imidazol-1-yl) ethanone-benzoyloxime (4o)

White crystal, yield 89%, m.p. 183.5–183.6 °C. ¹H NMR (400 MHz, DMSO *d*₆) δ (ppm): 8.410 (s, 1H), 8.174–8.153 (m, 2H), 7.787–7.749 (m, 1H), 7.713–7.691 (m, 2H), 7.630–7.595 (m, 4H), 5.866 (s, 2H), 2.253 (s, 3H). MS (ESI): 445.03 (C₁₉H₁₆BrN₄O₄,

[M+H]⁺). Anal. Calcd: C, 51.48; H, 3.41; N, 12.64%; Found: C, 51.56; H, 3.32; N, 12.72%.

4.2.16. 1-(4-Bromophenyl)-2-(2-methyl-4-nitro-1H-imidazol-1-yl)ethanone-(2-methoxy-benzoyl)oxime (**4p**)

White crystal, yield 85%, m.p. 156.9–157.2 °C. ¹H NMR (400 MHz, DMSO *d*₆) δ (ppm): 8.319 (m, 2H), 8.194 (s, 1H), 7.714–7.693 (m, 1H), 7.636–7.557 (m, 5H), 5.417 (s, 2H), 2.511–2.502 (m, 3H), 2.340 (s, 3H). MS (ESI): 475.04 (C₂₀H₁₈BrN₄O₅, [M+H]⁺). Anal. Calcd: C, 50.76; H, 3.62; N, 11.84%; Found: C, 50.84; H, 3.51; N, 11.96%.

4.2.17. 1-(4-Bromophenyl)-2-(2-methyl-4-nitro-1H-imidazol-1-yl)ethanone-(2-chloro-nicotinoyl)oxime (**4q**)

White crystal, yield 87%, m.p. 185.5–185.6 °C. ¹H NMR (400 MHz, DMSO *d*₆) δ (ppm): 8.761–8.732 (m, 1H), 8.166–8.153 (m, 2H), 7.839 (s, 1H), 7.636–7.625 (m, 2H), 7.589–7.576 (m, 2H), 5.034–5.017 (m, 2H), 2.342–2.339 (m, 3H). MS (ESI): 479.98 (C₁₈-H₁₄BrClN₅O₄, [M+H]⁺). Anal. Calcd: C, 45.16; H, 2.74; N, 14.63%; Found: C, 45.28; H, 2.65; N, 14.72%.

4.2.18. 1-(4-Bromophenyl)-2-(2-methyl-4-nitro-1H-imidazol-1-yl)ethanone-(6-chloro-nicotinoyl)oxime (**4r**)

White crystal, yield 91%, m.p. 180.4–180.5 °C. ¹H NMR (400 MHz, DMSO *d*₆) δ (ppm): 9.169–9.162 (m, 1H), 8.566–8.539 (m, 1H), 8.410 (s, 1H), 7.812–7.790 (m, 1H), 7.718–7.697 (m, 2H), 7.621–7.600 (m, 2H), 5.896 (s, 2H), 2.249 (s, 3H). MS (ESI): 479.98 (C₁₈H₁₄BrClN₅O₄, [M+H]⁺). Anal. Calcd: C, 45.16; H, 2.74; N, 14.63%; Found: C, 45.30; H, 2.62; N, 14.74%.

4.2.19. 1-(4-Bromophenyl)-2-(2-methyl-4-nitro-1H-imidazol-1-yl)ethanone-(6-methoxy-nicotinoyl)oxime (**4s**)

White crystal, yield 92%, m.p. 176.7–176.9 °C. ¹H NMR (400 MHz, DMSO *d*₆) δ (ppm): 9.030–9.025 (m, 1H), 8.399–8.365 (m, 1H), 7.707–7.685 (m, 2H), 7.616–7.579 (m, 3H), 7.013–7.014 (m, 1H), 5.875 (s, 1H), 5.417 (s, 1H), 2.510–2.502 (m, 3H), 2.251–2.244 (m, 3H). MS (ESI): 474.03 (C₁₉H₁₇BrN₅O₅, [M+H]⁺). Anal. Calcd: C, 48.12; H, 3.40; N, 14.77%; Found: C, 48.12; H, 3.40; N, 14.77%.

4.2.20. 1-(4-Bromophenyl)-2-(2-methyl-4-nitro-1H-imidazol-1-yl)ethanone-nicotinoyl oxime (**4t**)

White crystal, yield 92%, m.p. 179.3–180.2 °C. ¹H NMR (400 MHz, DMSO *d*₆) δ (ppm): 8.337–8.330 (m, 1H), 8.287–8.279 (m, 1H), 8.136 (m, 2H), 7.684–7.628 (m, 2H), 7.623–7.576 (m, 3H), 5.784 (s, 2H), 2.393–2.369 (m, 3H). MS (ESI): 444.02 (C₁₈H₁₅BrN₅O₄, [M+H]⁺). Anal. Calcd: C, 48.67; H, 3.18; N, 15.76%; Found: C, 48.67; H, 3.18; N, 15.76%.

4.2.21. 1-(4-Bromophenyl)-2-(2-methyl-4-nitro-1H-imidazol-1-yl)ethanone-isonicotinoyl oxime (**4u**)

White crystal, yield 95%, m.p. 166.3–166.6 °C. ¹H NMR (400 MHz, DMSO *d*₆) δ (ppm): 8.295–8.272 (m, 1H), 8.046–8.023 (m, 3H), 7.932–7.729 (m, 1H), 7.715–7.698 (m, 3H), 7.663–7.657 (m, 1H), 5.349 (s, 2H), 2.385–2.369 (m, 1H), 2.147 (s, 2H). MS (ESI): 444.02 (C₁₈H₁₅BrN₅O₄, [M+H]⁺). Anal. Calcd: C, 48.67; H, 3.18; N, 15.76%; Found: C, 48.74; H, 3.05; N, 15.63%.

4.2.22. 1-(4-Bromophenyl)-2-(2-methyl-4-nitro-1H-imidazol-1-yl)ethanone-(6-methyl-nicotinoyl)oxime (**4v**)

White crystal, yield 85%, m.p. 180.9–181.0 °C. ¹H NMR (400 MHz, DMSO *d*₆) δ (ppm): 8.518 (s, 1H), 8.411–8.385 (m, 1H), 8.195 (s, 1H), 7.712–7.691 (m, 1H), 7.621–7.502 (m, 4H), 5.882 (s, 1H), 5.417 (s, 1H), 2.607 (s, 1H), 2.510–2.502 (m, 2H), 2.251–2.245 (m, 3H). MS (ESI): 458.04 (C₁₉H₁₇BrN₅O₄, [M+H]⁺). Anal.

Calcd: C, 49.80; H, 3.52; N, 15.28%; Found: C, 49.92; H, 3.47; N, 15.17%.

4.3. Cell culture

A human hepatoma cell line (HepG2), human gastric cell line (MGC-803), carcinoma of cervix cell line (HeLa), human breast cell line (MCF-7) and human kidney epithelial cell (293T) were purchased from Nanjing Keygen Technology (Nanjing, China). Cells were maintained in Dulbecco's modified Eagle's medium (DMEM, Hyclone) (High Glucose) with L-glutamine supplemented with 10% foetal bovine serum (FBS, BI), 100 U/mL penicillin and 100 mg/mL streptomycin (Hyclone), and incubated at 37 °C in a humidified atmosphere containing 5% CO₂.

4.4. Anti-proliferation assay

The anticancer activities of the prepared compounds *in vitro* have been evaluated against MGC-803, MCF-7, HeLa and HepG2 cell lines. Target tumor cells were cultured in DMEM medium supplemented with 10% fetal bovine serum. After reaching a dilution of 1×10^5 cells mL⁻¹ with the medium, 100 μ L of the obtained cell suspension was added to each well of 96-well culture plates. Subsequently, incubation was performed at 37 °C in 5% CO₂ atmosphere for 48 h before the cytotoxicity assessment. Tested samples at preset concentrations were added to 6 wells with Erlotinib being employed as a positive reference. After 72 h exposure period, 25 μ L of PBS containing 2.5 mg mL⁻¹ of MTT was added to each well. After 4 h, the medium was replaced by 150 μ L DMSO to dissolve the purple formazan crystals produced. The absorbance at 570 nm of each well was measured with an ELISA plate reader. The data represented the mean of three independent experiments in triplicate and were expressed as means \pm SD. The IC₅₀ value was defined as the concentration at which 50% of the cells could survive.

4.5. PLK1-PBD inhibitor screening assay

The ability of compounds **4a–4v** to inhibitor PLK1-PBD was determined using fluorescence polarization screening assay.²⁵

4.6. Cell apoptosis assay

Approximately 10^5 cells/well were plated in a 24-well plate and allowed to adhere. Subsequently, the medium was replaced with fresh culture medium containing compound **4v** at final concentrations of 0, 0.01, 0.06 and 0.12 μ M. Non-treated wells received an equivalent volume of ethanol (<0.1%). After 24 h, cells were trypsinized, washed in PBS and centrifuged at 2000 rpm for 5 min. The pellet was resuspended in 500 μ L staining solution (containing 5 μ L AnnexinV-FITC and 5 μ L PI in Binding Buffer), mixed gently and incubated for 15 min at room temperature in dark. The samples were then analyzed by a FACSCalibur flow cytometer (Becton Dickinson, San Jose, CA, USA).

4.7. Scaffold modification

Scaffold modification was achieved with the module Grow Scaffold in Discovery Studio (version 3.5). Following the protocol, the scaffold was docked into PLK1 (PDB code: 4HCO) binding site beforehand. The nitroimidazole-oxime scaffold were then marked as sites to be substituted. After calculation, modified molecules were produced to generate a library of small molecules.

4.8. Docking simulation

The three-dimensional structures of the aforementioned compounds were constructed using Chem. 3D ultra 11.0 software [Chemical Structure Drawing Standard; Cambridge Soft corporation, USA (2009)], then they were energetically minimized by using MOPAC with 100 iterations and minimum RMS gradient of 0.10. The Gasteiger-Hückel charges of ligands were assigned. Molecular docking of the compounds binding the three-dimensional X-ray structure of PLK1 (PDB code: 4HCO) was carried out using Discovery Studio (version 3.5) as implemented through the graphical user interface DS-CDOCKER protocol. For enzyme preparation, the hydrogen atoms were added with the pH of the protein in the range of 6.5–8.5. CDOCKER is an implementation of a CHAR Mm based molecular docking tool using a rigid receptor. It includes the following steps:

- (1) A series of ligand conformations are generated using high temperature molecular dynamics with different random seeds.
- (2) Random orientations of the conformations are generated by translating the center of the ligand to a specified position within the receptor active site, and making a series of random rotations. A softened energy is calculated and the orientation is kept when it is less than a specified limit. This process repeats until either the desired number of low-energy orientations is obtained, or the test times of bad orientations reached the maximum number.
- (3) Each orientation is subjected to simulated annealing molecular dynamics. The temperature is heated up to a high temperature then cooled to the target temperature. A final energy minimization of the ligand in the rigid receptor using non-softened potential is performed.
- (4) For each of the final pose, the CHARMM energy (interaction energy plus ligand strain) and the interaction energy alone are figured out. The poses are sorted according to CHARMM energy and the top scoring (most negative, thus favorable to binding) poses are retained. The whole PLK1-PBD domain defined as a receptor. CHARMM was selected as the force field. The molecular docking was performed with a simulated annealing method. The heating steps were 2000 with 700 of heating target temperature. The cooling steps were 5000 with 300 cooling target temperature. Ten molecular docking poses saved for each ligand were ranked according to their dock score function. The pose with the highest -CDOCKER energy was chosen as the most suitable pose.

Acknowledgments

This work is granted by Natural Science Foundation of Jiangsu Province (BK20160570), and Jiangsu Planned Projects for Postdoctoral Research Funds (1601041A).

References

1. Archambault V, Lepine G, Kachaner D. Understanding the Polo kinase machine. *Oncogene*. 2015;34:4799–4807.
2. Schuldt A. Cell division: a timely exit for PLK1. *Nat Rev Mol Cell Biol*. 2013;14:194–195.
3. McInnes C, Wyatt MD. PLK1 as an oncology target: current status and future potential. *Drug Discovery Today*. 2011;16:619–625.
4. Murugan RN, Park JE, Kim EH, et al. Plk1-targeted small molecule inhibitors: molecular basis for their potency and specificity. *Mol Cells*. 2011;32:209–220.
5. Garuti L, Roberti M, Bottegoni G. Polo-like kinases inhibitors. *Curr Med Chem*. 2012;19:3937–3948.
6. Li S, Zhang Y, Xu W. Developments of polo-like kinase 1 (Plk1) inhibitors as anti-cancer agents. *Mini-Rev Med Chem*. 2013;13:2014–2025.
7. Noble ME, Endicott JA, Johnson LN. Protein kinase inhibitors: insights into drug design from structure. *Science*. 2004;303:1800–1805.
8. DeLano WL, Ultsch MH, deVos AM, Wells JA. Convergent solutions to binding at a protein-protein interface. *Science*. 2000;287:1279–1283.
9. Lee KS, Burke TR, Park JE, et al. Recent advances and new strategies in targeting Plk1 for anticancer therapy. *Trends Pharmacol Sci*. 2015;36:858–877.
10. Xu J, Shen C, Wang T, et al. Structural basis for the inhibition of Polo-like kinase 1. *Nat Struct Mol Biol*. 2013;20:1047–1053.
11. Elia AE, Cantley LC, Yaffe MB. Proteomic screen finds pSer/pThr-binding domain localizing Plk1 to mitotic substrates. *Science*. 2003;299:1228–1231.
12. Yun SM, Moulaei T, Lim D, et al. Structural and functional analyses of minimal phosphopeptides targeting the polo-box domain of polo-like kinase 1. *Nat Struct Mol Biol*. 2009;16:876–882.
13. Liu F, Park JE, Qian WJ, et al. Serendipitous alkylation of a Plk1 ligand uncovers a new binding channel. *Nat Chem Biol*. 2011;7:595–601.
14. Murugan RN, Park JE, Lim D, et al. Development of cyclic peptomer inhibitors targeting the polo-box domain of polo-like kinase 1. *Bioorg Med Chem*. 2013;21:2623–2634.
15. Kim SM, Chae MK, Lee C, et al. Enhanced cellular uptake of a TAT-conjugated peptide inhibitor targeting the polo-box domain of polo-like kinase 1. *Amino Acids*. 2014;46:2595–2603.
16. Ahn M, Han YH, Park JE, et al. A new class of peptidomimetics targeting the polo-box domain of polo-like kinase 1. *J Med Chem*. 2014;58:294–304.
17. Reindl W, Yuan J, Krämer A, et al. Inhibition of polo-like kinase 1 by blocking polo-box domain-dependent protein-protein interactions. *Chem Biol*. 2008;15:459–466.
18. Reindl W, Yuan J, Krämer A, et al. A pan-specific inhibitor of the polo-box domains of polo-like kinases arrests cancer cells in mitosis. *ChemBioChem*. 2009;10:1145–1148.
19. Li L, Wang X, Chen J, et al. The natural product Aristolactam AIIIa as a new ligand targeting the polo-box domain of polo-like kinase 1 potently inhibits cancer cell proliferation. *Acta Pharm Sin*. 2009;30:1443–1453.
20. Shan HM, Shi Y, Quan J. Identification of green tea catechins as potent inhibitors of the polo-box domain of polo-like kinase 1. *ChemMedChem*. 2015;10:158–163.
21. Srinivasrao G, Park JE, Kim S, et al. Design and synthesis of a cell-permeable, drug-like small molecule inhibitor targeting the polo-box domain of polo-like kinase 1. *PLoS One*. 2014;9:e107432.
22. Chen DX, Huang J, Liu M, Xu YG, Jiang C. Design, synthesis, and evaluation of non-ATP-competitive small-molecule polo-like kinase 1 (PLK1) inhibitors. *Arch Pharm Chem Life Sci*. 2015;348:2–9.
23. Sun J, Lv PC, Guo FJ, et al. Aromatic diacylhydrazine derivatives as a new class of polo-like kinase 1 (PLK1) inhibitors. *Eur J Med Chem*. 2014;81:420–426.
24. Yin Z, Song YL, Rehse PH. Thymoquinone blocks pSer/pThr recognition by Plk1 Polo-box domain as a phosphate mimic. *ACS Chem Biol*. 2013;8:303–308.
25. Chen YY, Zhang J, Li DS, Jiang JD, Wang YC, Si SY. Identification of a novel Polo-like kinase 1 inhibitor that specifically blocks the functions of Polo-Box domain. *Oncotarget*. 2017;8:1234–1246.